CHALMERS

Investigation of sedimentation behaviour of micro crystalline cellulose

Master's Thesis in the Master Degree Programme, Chemical Engineering

EDUARD LAGUARDA MARTINEZ

Department of Chemical and Biological Engineering
Division of Forest Products and Chemical Engineering
CHALMERS UNIVERSITY OF TECHNOLOGY
Göteborg, Sweden, 2012

Investigation of sedimentation behaviour of micro crystalline cellulose

Relating particle-to-particle interaction to sedimentation behaviour

EDUARD LAGUARDA MARTINEZ

Department of Chemical and Biological Engineering
CHALMERS UNIVERSITY OF TECHNOLOGY
Göteborg, Sweden 2012

Investigation of sedimentation behavior of micro crystalline cellulose
Relating particle-to-particle interaction

Department of Chemical and Biological Engineering
Chalmers University of Technology
SE-412 Göteborg
Sweden
Telephone +46 (0)31-772 1000

Investigation of sedimentation behaviour of micro crystalline cellulose

EDUARD LAGUARDA MARTINEZ
Department of Chemical and Biological Engineering
Chalmers University of Technology

ABSTRACT

Batch settling is a widely used method to separate a flocculated suspension into concentrated sediment and a clear liquid. Experimental and theoretical studies of this process have been published for almost a century due to its importance in separation processes.

Fundamental aspects of sedimentation and suspension flows include properties of suspensions (concentration and viscosity); individual particles (particle size and shape, particle-particle interaction, surface charge); and sediments (permeability, porosity and compressibility).

The investigated material, MCC, is of great interesting for several different applications, e.g. in the food and pharmaceutical industry.

Hence, this work investigates the sedimentation process of micro crystalline cellulose in order to understand its behaviour considering the different conditions set out.

Based on the results obtained in this work the following conclusions can be drawn: both the sedimentation behaviour and the compressibility of the sediment are affected by the surface charge of the MCC particles; finally, the solidosity of the sediment is as a function of pH.

Keywords: concentration, settling rate, suspension, solid volume fraction, particle-particle interaction, sedimentation.

Acknowledgements

The author would like to thank:

- *My supervisor Ph. D Student Tuve Mattsson for his assistance in conducting with both the experiment and my Master's Thesis. Also for his constant help and encouragement, his valuable advices were really useful.*
- *My co-supervisor Dr. Maria Sedin for providing me new ideas related with the theory used and for our interesting meetings about MCC (micro crystalline cellulose).*
- *The research group in solid-liquid-filtration at Forest Productions & Chemical Engineering, in whose laboratories the experiment was carried out, for providing me the chance of lifetime.*
- *All members of the department for having a good time among them.*

Contents

1 Introduction

1.1 Sedimentation process

Sedimentation as a means of separating solids from liquids is used in a wide range of industries: sewage treatment, mineral and pharmaceutical industries to name a few.

The settling process of a flocculent suspension gives rise to three different and well-distinguishable zones (*Fig. 1.1*). From top to bottom; a thin layer located at the surface called *clear water zone*; another zone in which the suspension is present at its *initial concentration*; and a *compression zone* initially located at the bottom whose height increases during the process.

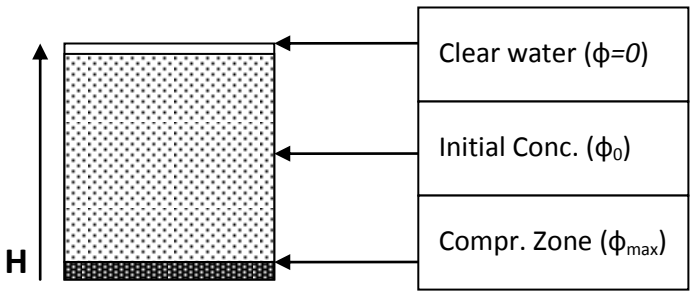

Figure 1.1. Initial sedimentation process.

1.2 Free settling

Many gravitational sedimentation experiments have been carried out to determine relationship between settling velocity and particle size. A unique relationship has been found between drag factor and Reynolds number. This relationship reduces to a simple equation, the Stokes' equation, which is valid at low Reynolds numbers. Thus, at low Reynolds numbers the settling velocity defines an equivalent Stokes' diameter which, for a homogeneous spherical particle, is its physical diameter.

At low Reynolds number the flow is said to be laminar. As the Reynolds number increases, turbulence sets in leading to increased drag on the particle so that it settles at a lower velocity than predicted by Stokes' equation.

Gravitational sedimentation process is, however, considered to be within the laminar range so that Stokes' relationship has been used to determine particle size.

Gravitational sedimentation methods of particle size determination are based on the settling behaviour of a single sphere, under gravity, in a fluid. In contrast, a related technique named centrifugation is based on an artificial field.

1.3 Hindered settling

G.J. Kynch [1] suggested a mathematical description of the batch sedimentation of an initially homogeneous suspension considering only the hindered effect. Therefore, in the hindered settling range, the settling rate depends only on the solids concentration and this relationship can also be applied when changing the solids concentration in batch testing.

It is known that gravity sedimentation is inherently unstable and particles tend to settle in a random manner as a result of the effects related with the mentioned properties above.

1.4 The scope of the thesis

This thesis investigates MCC (micro crystalline cellulose) particles settling under the influence of gravity and how the sedimentation process is affected by particle-to-particle interaction by altering the surface charge on particles. In Chapter 2 an overview of the used theory is presented. Chapter 3 describes the experimental equipment as well as a characterization of the materials used. The results are gathered and discussed in Chapter 4. Finally, conclusions are presented at the end of this paper in Chapter 5. A personal point of view is found in Chapter 6 called *Future work* and an annex is added in Chapter 7 which includes the programs used during this work.

2 Theory

2.1 Stokes' law equation

In 1851 Stokes obtained a theoretical equation (1) for the drag force acting on a single spherical particle moving relative to a continuous fluid.

$$F_D = 3\mu\pi ud \tag{1}$$

Where F_D is the drag force, μ is the viscosity of the fluid, u is the relative velocity and d is the diameter of the sphere.

The fluid was assumed to extend infinite and the relative velocity low so that inertia of the particle could be neglected. At high velocities the drag increases above what is predicted by Stokes' equation, due to the onset of turbulence, leading to a slower settling speed than the law predicts [9].

As the particle concentration is increased, interparticle interactions become important [5].

2.1.1 Relationships between settling velocity and particle size

When a particle falls under gravity in a fluid, it is acted upon by three forces; a gravitational force W acting downwards; a buoyant force U and a drag force F_D both acting upwards [3].

$$W - U - F_D = mg - m'g - F_D = m\frac{du}{dt} \tag{2}$$

Where m is the mass of the particle, m' is the mass of the same volume of fluid, u is the particle velocity and g is the acceleration due to gravity.

For a sphere of diameter d and density ρ_s falling in a fluid of density ρ_f, the equation of motion becomes as follows once the particle reaches the terminal velocity, i.e. steady state.

$$\frac{\partial u}{\partial t} = 0 \tag{3}$$

$$F_D = mg - m'g \tag{4}$$

$$F_D = \frac{\pi}{6}(\rho_s - \rho_f)gd^3 \tag{5}$$

Therefore, the drag coefficient (*CD*) can be known as follows:

$$CD = \frac{\text{drag force}}{\text{cross-sectional area of the sphere x dynamic pressure on the particle}} \quad (6)$$

$$F_D = CD\ x\ \frac{\pi d^2}{4}\ x\ \frac{\rho_f u^2}{2} \quad (7)$$

Combining equations (5) and (7) gives:

$$CD = \frac{4}{3}\frac{(\rho_s - \rho_f)}{\rho_f}\frac{gd}{u^2} \quad (8)$$

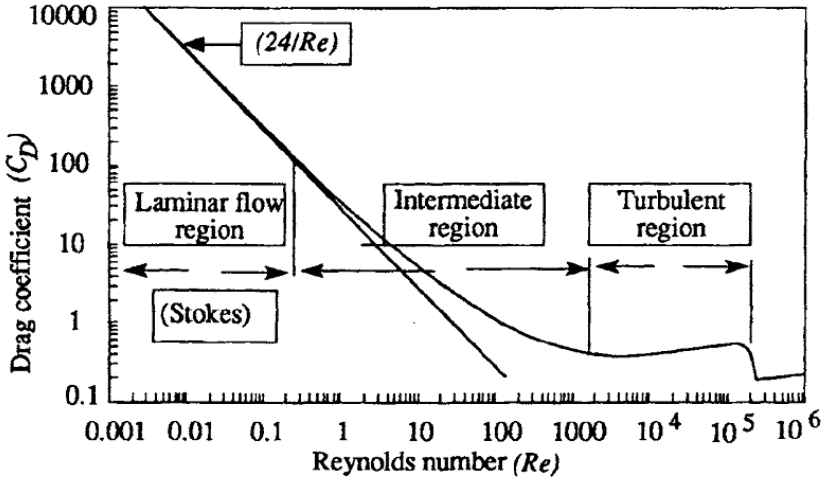

Figure 2.1. Experimental relationship between drag coefficient and Reynolds number for a sphere settling in a liquid Extracted from [3].

Dimensionless analysis of the general problem of particle motion under equilibrium conditions gives a unique relationship between two dimensionless groups, drag coefficient and Reynolds number.

From *Figure 2.1* it can be observed that, as the Reynolds number approaches zero, *CDxRe* approaches 24, i.e. in the limit.

$$CD = \frac{24}{Re} \quad (9)$$

In the laminar flow region, in which is supposed that the sedimentation experiments were carried out, can be used:

$$F_D = 3\pi d\mu u_{St} \tag{10}$$

Then, inserting equation (10) in equation (5) gives the relationship between the particle diameter and its Stokes' velocity:

$$d = \sqrt{\frac{18\mu u_{St}}{(\rho_s - \rho_f)g}} \tag{11}$$

Where u_{St} is the terminal velocity for a sphere of diameter d in the laminar flow region. Equation (11) can be used to determine u_{St} for a given particle diameter, provided that Stokes' equation is applicable.

2.2 Concentration effects

Stokes' equation (1) applies to the settling of a single spherical particle. This requirement is never fulfilled in sedimentation batch testing where particles are separated by finite distances and mutually affect each other. Two cases of sedimentation processes should be mentioned: an assembly of particles which completely fills the fluid and, in contrast, a cluster of particles or agglomerate.

The descent of a single particle creates a velocity field which tends to increase the velocity of nearby particles. To balance this, the downward motion of the particle must be compensated for an equal volume upflow.

Regarding batch experiments, where a great amount of particles settle randomly, if the particles are not uniformly distributed the effect is a net increase in settling velocity since the return flow will predominate in particle sparse regions. In contrast, a system of uniformly distributed particles will be retarded as a result of a net increase in fluid-particle friction forces named *shear forces*, leading to a decreased settling rate [3]. *Figure 2.2* exhibits both modes of sedimentation.

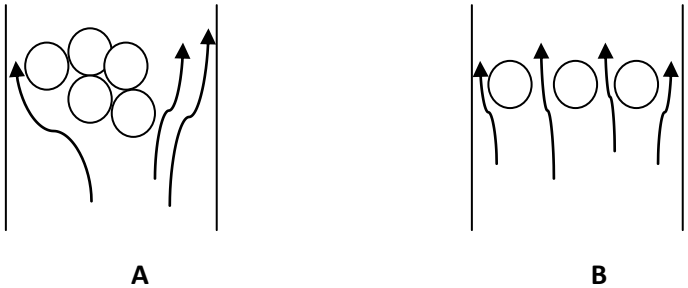

Figure 2.2. A: a cluster of particles; B: uniformly distributed particles. Arrows show the return flow going through particles.

2.2.1 Hindered settling

At very low concentrations particles settle independently, under no influence of other particles and, under laminar flow conditions, Stokes' law is thus valid. At higher concentrations (approx. ϕ>0.002) particle-particle interaction occur which, on average, should lead to reduced settling rates. At very high concentrations particles tend to settle *en masse* leading to an increased settling rate above what is initially expected.

The interface between suspension and clear liquid is sharp for a single sphere but more diffuse for powders with a wide size range which, and in some cases, form more than one interface. This phenomenon is due to fines being swept out of the bulk of the suspension by return flow of liquid displaced by sediment solids and, therefore, that phenomenon creates a suspension of fines over the main suspension; the fines supernatant being, in turn, subject to hindered settling.

2.3 Kynch's theory of sedimentation

Kynch's sedimentation theory is a well-known mathematical model for the one-dimensional batch and continuous sedimentation of ideal suspensions of monosized spheres under the influence of gravity. The theory assumes that the drift velocity (terminal velocity) of particles in dispersion is determined by the local particle concentration only. The relationship between the two variables can be deduced from observations on the velocity of the top of the dispersion. It is shown that discontinuous changes in the particle density can occur under the stated conditions in elsewhere [1].

Assume that batch sedimentation is performed in a vessel of height *H* and with constant cross sectional area. Let *ϕ(h,t)* be the concentration (volume fraction) of solids at height *h*, measured from the bottom, and at time *t*.

The constitutive assumption by Kynch is assumed to hold, i.e. the settling velocity of the particles depends only on the local concentration [1].

$$v_S = v_S(\emptyset) \geq 0 \tag{12}$$

The used convention is that the settling velocity and flux are positive in the downward direction. A mass balance over the system yields:

$$\frac{\partial \emptyset}{\partial t} + \frac{\partial f_{bk}}{dh} = 0\,; \quad 0 \leq h \leq H \;\;,\;\; 0 \leq t \tag{11}$$

Where f_{bk} is the Kynch's batch flux density function and v_S is the solid-phase velocity.

Hence, Kynch's batch flux density function takes the form:

$$f_{bk} = v_s \emptyset \tag{12}$$

The initial condition for an initially homogeneous suspension (*t=0*) is:

$$\emptyset(h, 0) = \emptyset_0 \quad \text{for } 0 \leq h \leq H \tag{13}$$

Where it is assumed that the function $f_{bk}=\phi v_s(\phi)$ satisfies $f_{bk}(\phi)=0$ for $\phi \leq 0$ or $\phi \geq \phi_{max}$ and $f_{bk}<0$ for $0<\phi<\phi_{max}$, where ϕ_{max} is the maximum solids concentration.

2.4 Richardson and Zaki's two-parameter equation

To describe the batch-settling velocities of particles in real suspension the following two-parameter equation was proposed by Richardson and Zaki (1954) [9]:

$$f_{bk} = u_\infty \emptyset (1 - \emptyset)^n \tag{14}$$

Michaels and Bolger [8] proposed the following three-parameter equation owing to the settling velocity becomes zero at a maximum concentration, not at the solid concentration $\phi=1$.

$$f_{bk} = u_\infty \emptyset \left(1 - {\emptyset}/{\emptyset_{max}}\right)^n \tag{15}$$

$$\frac{u_s}{u_\infty} = \left(1 - {\emptyset}/{\emptyset_{\max}}\right)^n \tag{16}$$

Where $n=4.65$ turned out to be suitable for rigid spheres and u_∞ is supposed to be the terminal velocity calculated by Stokes' equation (u_{st}). This model is empirical and arose from experimentation and accurate observation.

2.5 Vesilind's equation

In contrast, Vesilind's equation [10] is applied to a situation in which the slurry does not present a maximum possible concentration in a time frame of the process. This model is empirical and is employed after experimental observations. Vesilind's equation takes the form:

$$v_S(\emptyset) = v_0 e^{-n'\emptyset} \tag{17}$$

Where both v_0 and n' are parameters to be determined experimentally.

2.6 Batch sedimentation model

In order to ease the analysis of the sedimentation experiment, one-dimension modelling of such process is based on the following assumptions which are briefly presented.

- Velocity of solids particles depends only on the local suspended solids concentration (v_s (ϕ)).
- Only vertical movement of particles is considered and the horizontal gradients in suspended solids concentration are negligible.
- Movement of solid particles results only from gravitational settling.
- Wall effects can be ignored.
- The particles are of the same size and shape and approximated with an equivalent sphere.
- The sediment can be classified as incompressible.

2.7 Compressible sediment

Buscall and White [27] proposed a model considering the flocculated slurry as a purely plastic body that possesses a yield stress (P_y(ϕ)). If the local pressure of sediment exceeds P_y, the network structure would yield. The proposed constitutive equation takes the form:

$$\frac{\partial \emptyset}{\partial t} = k(\emptyset, P_S)\left(P_S - P_y(\emptyset)\right) \tag{18}$$

If $P > P_y$(ϕ). Otherwise, the sediment would be incompressible:

$$\frac{\partial \emptyset}{\partial t} = 0 \tag{19}$$

Where k is called the dynamic compressibility.

2.8 Concentrations measurements

Consider a sedimentation cell of width d_y measured in the direction of the light beam, containing the suspension under analysis (*Fig. 2.3*).

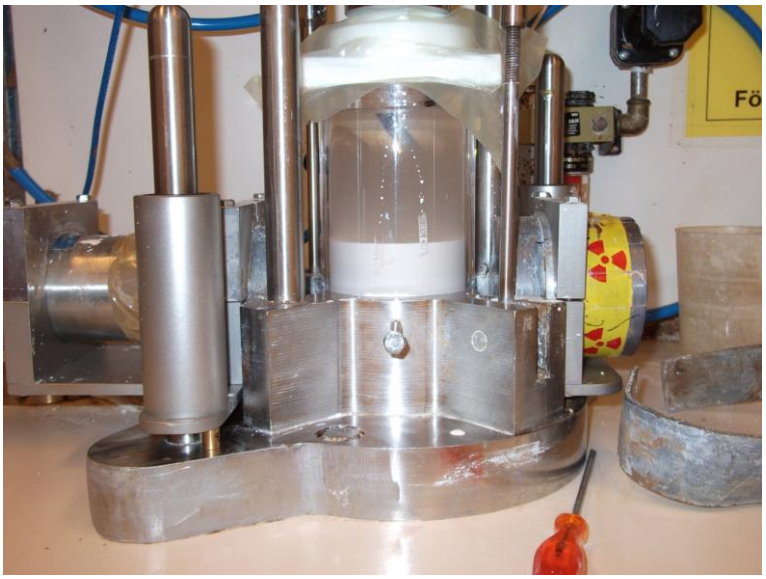

Figure 2.3.γ-source and the sedimentation cell.

Let the light intensity emerged from an empty cell be I_0 and the emerging light flux from the filled cell be I. Therefore, these γ-attenuation measurements can be used to determine the solid volume fraction for a fixed height of the sedimentation cell during the experiment. Thus, the Beer-Lambert law takes the form:

$$I = I_0 e^{-(\mu_S \emptyset + \mu_l (1-\emptyset)) d_y} \tag{20}$$

Where μ is the attenuation constant for the liquid (l) and the solid (s). The solid phase has a higher attenuation due to its capability of absorbing larger amounts of ϒ-rays than distillate water. Finally, d_y is the path followed by the γ-rays.

3 Material and equipment set up

The following sections describe the model material used, the methods employed and the experimental equipment with which the experiments were carried out.

3.1 Material

The material used was Avicel® PH-105 microcrystalline cellulose manufactured by FMC Corporation. *Figure 3.1* shows a SEM photograph of the model material employed.

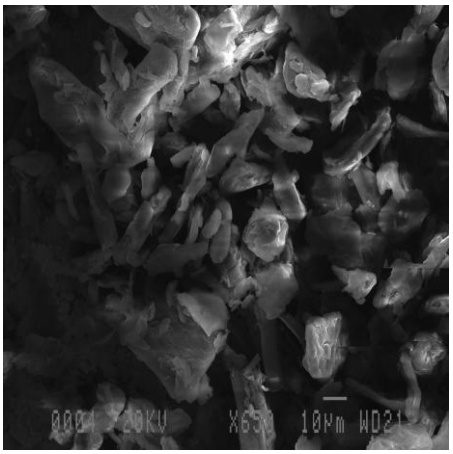

Figure 3.1. SEM photograph of AVICEL PH105 under acidic conditions.

Microcrystalline cellulose is prepared from dissolving pulp of high purity. The native cellulose chain is built up of D-glucopyranose units joined by β-1,4-linkages, chains ranging up to several thousand units. The cellulose materials consist of amorphous cellulose areas, in addition to well ordered crystalline regions. During the manufacture of microcrystalline cellulose, accessible amorphous cellulose areas are hydrolysed away and the chain length, measured as the degree of polymerization of the cellulose, falls to a degree of polymerization value around some hundreds. When the fibrous structures are broken down, the resulting cellulose particles are washed and spray dried into a cellulose powder (ρ=1.56 g/cm^3).

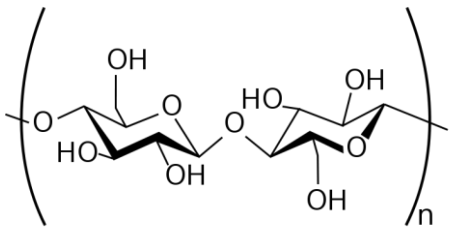

Figure 3.2. Cellulose unit.

3.1.1 Particle characterization

The microcrystalline cellulose particles were characterised by size for each pH level. A SEM picture of the particles is shown in *Fig. 3.1*. The slurry used in the particle characterization was

ultrasonic treated in order to avoid agglomeration of particles in the size determination. The *particle diameter* [1]is given in *Table 3.1* and was determined using laser diffraction.

Table 3.1. Particle characterization.

pH	$D_{(0.1)}$(µm)	$D_{(0.5)}$(µm)	$D_{(0.9)}$(µm)
2.9	10.6	25.3	52.6
6.7	9.4	21.1	42.6
9.4	10.9	22.3	43.2

The average diameter is considered to be $D_{(0.5)}$ while $D_{(0.1)}$ and $D_{(0.9)}$ correspond to a diameter where 10 and 90 volume %, respectively, are smaller than the value stated .

3.1.2 Surface properties

To understand how MCC particles interact during sedimentation, a brief discussion about surface charge of the MCC is presented.

To start with, when cellulose is brought into contact with an aqueous electrolyte solution, the colloidal surface acquires an electric surface charge through several mechanisms which are basically dissociation (ionization) of surface functional groups; and adsorption of ions from solution. The effects are dependent on, among other variables, the zeta potentials of the surface and suspended ions. The particle properties are dependent on the degree of ionization and, therefore, the pH level of the aqueous solution as it can be seen in *Fig. 3.3*. For Avicel PH-105, titrations with a linear polyDADMAC with a known change density indicated that particles had a somewhat negative charge: in the range of -1 µeq g^{-1} at pH 6.3/9.3 and close to zero at pH 2.9.

The surface charge is compensated by counter-ions in the suspension surrounding close to the surface, forming a shielding layer named *electrical double layer*. This shielding layer stabilises agglomerates.

[1] The particle diameter is assumed to be as if the particle's shape is spherical.

Figure 3.3 shows the results obtained during titrations.

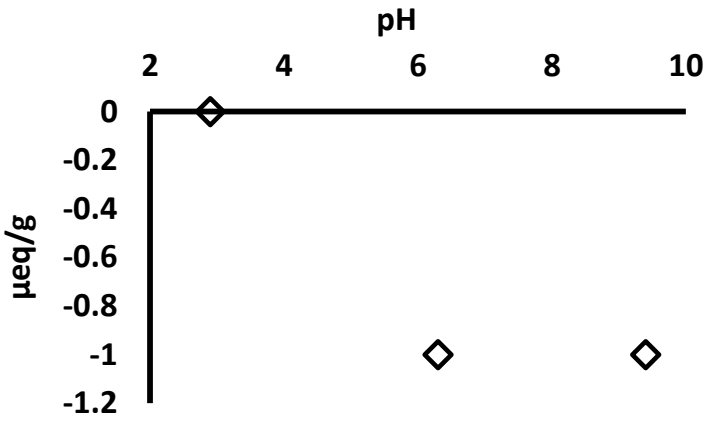

Figure 3.3. Surface charge.

Surface charge turned out to be more negative (anionic) with increasing pH due to increased dissociation of hydrogen bonds and remains constant above pH equal to 6.4 due to their complete dissociation (*Fig. 3.3*). The results obtained are important in order to decide which pH levels are interesting to investigate.

Agglomerates stability is often discussed based on two forces, an attractive Van der Waals force and a repulsive force due to the electrical double layer. The sum of the two potentials determines the stability between the particle-particle interactions and, as a result of these interactions, the stability of agglomerates. The *shear layer* is located between the surface charge and the ions surrounding close to the particle surface. The distance that the layer takes from the outer surface corresponds to when repulsive and attractive forces remain equalized.

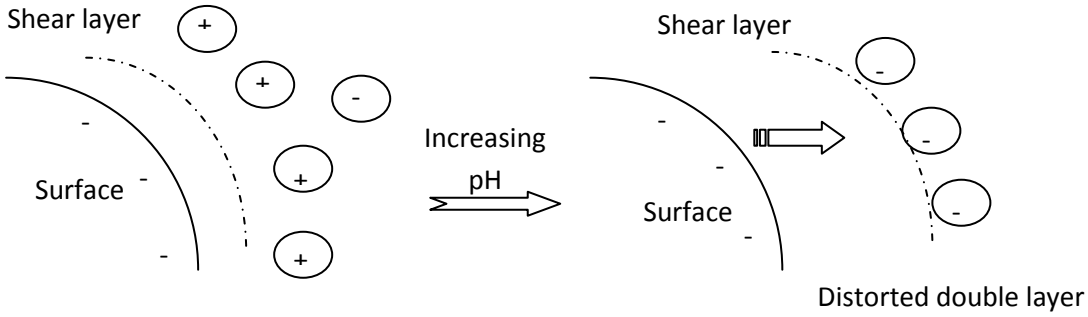

Figure 3.4 It is shown how the double layer gets stressed from neutral pH to basic pH arising from the repulsion forces owing to the increased hydroxide concentration.

The mentioned double layer (within high pH values) is distorted when the particles settle under gravity with the result in an electrical field is set up which opposes motion [24]. The distorted layer phenomenon arises from hydrodynamic diffusion effects while the double layer appears as a result of dynamic charges.

Hence, the study of the presence of electrical charges is one of great importance in order to predict the behaviour during the sedimentation process. The behaviour of polymeric surfaces is discussed in detail elsewhere [23-25].

3.2 Experimental equipment

3.2.1 The sedimentation method

The following method was used during experiments. Concentration changes were determined within a settling suspension, at predetermined times and known heights, by means of a column. This method is versatile, since it can handle any powder which can be dispersed in a liquid, and the apparatus is inexpensive. The analysis is however time consuming and operator intensive.

After agitation, a finite time is required before the particles commence to settle uniformly, but this is much greater than the time the particles are accelerating to a constant velocity, known as the terminal velocity or drift velocity, under gravitational force.

During this work, two different sedimentation columns were used

3.2.2 Sedimentation equipment

Both columns used are named as follows: *set up 1* with which enables to observe the height of the uppermost layer whilst the experiment was being carried out; and *set up 2* to measure the solid volume fraction at different levels by means of ϒ-attenuation.

3.2.2.1 Set up 1

A cylinder 30 cm in height whose inner diameter is 4.5 cm was used to observe the height of the uppermost layer. A ruler is attached along the tube to facilitate the estimation of the height of the bottom of the clear phase as a function of time.

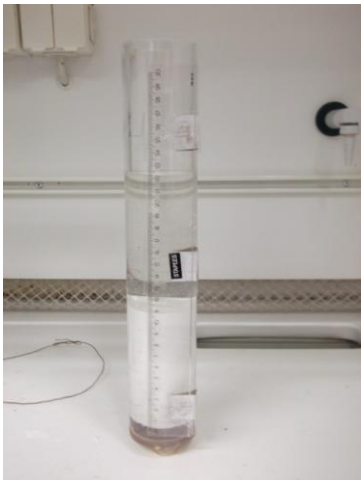

Figure 3.5. Lab. Equipment: set up 1.

3.2.2.2 Set up 2

Set up 2 comprises a cylinder 11.5 cm in height and its inner diameter is 6 cm whose bottom consists of a perforated plastic cover, which serves as a support for the retaining membrane. A 5-stacked membrane is put on the bottom of the sedimentation cell so as to avoid any leak. The test filtration apparatus comprises of a piston press which pushes down towards the sedimentation cell to seal it.

Figure 3.6. Lab. Equipment: set up 2.

The solid volume fraction could be calculated using the Beer-Lambert law for both phases, the liquid (l) and the solid (s):

$$-ln\left(\frac{\eta_\gamma}{\eta_{\gamma,0}}\right) = \mu_{\gamma,l} d_\gamma + \left(\mu_{\gamma,s} - \mu_{\gamma,l}\right) d_\gamma \emptyset \qquad (21)$$

Where η_Υ and $\eta_{\Upsilon,0}$ are the number of counts for the filled cell and for the empty cell, respectively; and μ_s and μ_l are the attenuation coefficients determined by calibration. The former was obtained from a dried cellulose cake whose value was 28.9 m^{-1}; and the latter from distillate water whose value was 19.8 m^{-1}.Finally, d_γ is the average path of the ϒ-attenuation within the filter cell which is 6 cm.

3.3 Experimental conditions

3.3.1 Sedimentation set-up

Sedimentation experiments have been performed with six different slurries; with varying solid volume concentration and pH.

The two solid volume concentrations were investigated: 5% (*low concentration*) and another of 10% (*high concentration*). For each concentration, three different slurries were prepared at pH values of 2.9, 6.7 and 9.4, respectively.

In order to prepare each slurry, the pH was adjusted using NaOH for high pH values (a solution of sodium hydroxide 1 M was used to reach a pH of 9.4). Likewise, HCl for low pH values (a solution of hydrochloric acid 0.5 M was used to reach a pH of 3).

Before experiments, the slurry was vigorously stirred and a specific volume was poured into the sedimentation column. Distillate water was used as the fluid (aqueous suspension).

All experiments were carried out at the same temperature, 21^{o}C.

3.3.2 Set up 1 test

Once the slurry was prepared and poured into *set up 1*, the height of the interface was registered as a function of time. *Figure 4.1* shows the sedimentation profile for each experiment which was conducted within that vessel.

3.3.3 Set up 2 test

The same suspensions and method as described for *set up 1* was used for *set up 2*. In addition, some tape was used to seal the cell in order to minimize evaporation. After that, the ϒ-attenuation equipment started collecting all the data in the computer whilst the experiment was being carried out, i.e. the *transitory state*. Finally, the column was checked at specific height yielding the profile of the entire cell. *Figures 4.6, 4.7, 4.8* and *4.9* show the values obtained.

4 Results and discussion

The results obtained during this work are presented in the following sections.

4.1 Particle characterization

Particles were treated and analysed using ultrasound to break agglomerations up. Nonetheless, no big difference was found related with particle diameter within the different samples used as it could be seen in *Table 3.1*. It is thought that the slightly difference among each other could reside in the time that the sample was under the ultrasonic treatment and the efficiency during the analysis.

4.2 Settling rate

4.2.1 Batch settling

Figure 4.1 shows the different settling rates dependency on both the pH and the solid concentration in the slurry from *set up 1*.

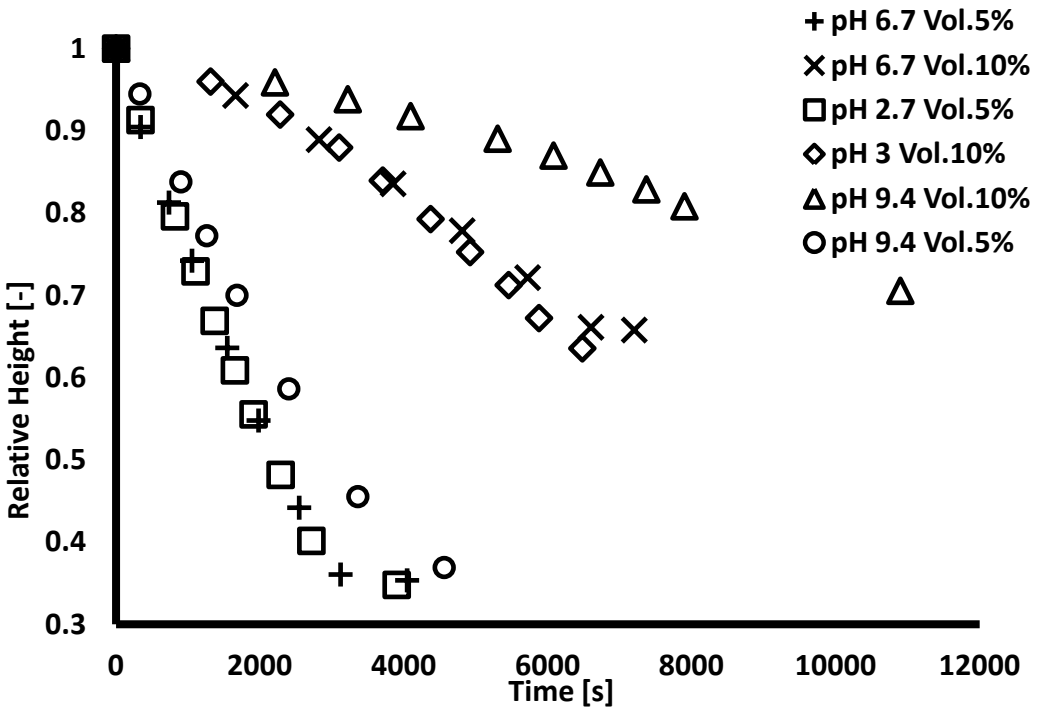

Figure 4.1. Settling plot. The relative height is defined as H/H_0.

To understand how the experimental conditions affect the sedimentation process and, more specifically, each particle, a brief discuss follows.

Overall, the settling rates obtained are qualitatively predictable. As was expected for low level of concentration, higher settling rates were observed compared to the high concentration level. One explanation might be as the concentration increases, the particles come into closer

contact; there is increased interaction and they can no longer be treated as individual units. Thus, the higher the concentration, the more pronounced this effect becomes.

As can be seen in *Figure 4.1*, settling rates are quite similar within the range of acid and neutral pH for a given concentration but not for high pH which exhibits, however, a different behaviour.

Furthermore, the agglomerates, which are built up within acidic environments or even neutral environments, exhibit a more stable structure. It might be due to the presence of hydronium onto the surface through which hydrogen bonds are made, strengthen in this way the agglomerate's structure. Otherwise, it is thought the double layer would not get stabilized by the lack of presence of counter-ions. As a result, increased intra-particle interactions would arise from the repulsive forces among negative charges leading to a particle governed by hydrodynamic diffusions. It is considered this sort of forces are the responsible for the agglomerates breakdown. It means settling more randomly and, in consequence, slower. Thus, high-pH environments lead to set a stressed double layer up which opposes motion.

Regarding the settling rate, it is likely that the small difference that appears between the high-concentration-and-low-pH and the high-concentration-and-neutral-pH curves is owing to concentration effects. For lower pH, agglomerates appear to be more stable and they could endure the multiple collisions while on the other hand, for neutral pH, collisions lead to break up agglomerates in smaller particles and the settling rate decreases.

During the last experiment, which was the low concentration at high pH, a diffuse layer could be discovered between the colloidal suspension and the compression zone. It is thought to consist of swept fine particles by flocculated flocs, which gradually disappeared whilst the experiment was being carried out. Nonetheless, this behaviour was not displayed at high concentration. One possible explanation of the two different behaviours might be the particle-particle interaction; the finer powder could not settle as the bigger particles due to the distorted double layer which response is much stronger than the drag force applied downwards for smaller particles; in contrast, for higher concentrations this finer powder get dragged by the influence of surrounding agglomerates. Hence, it could be said that for high concentrations mechanical forces become much more important than the chemical forces.

4.2.2 Modes of sedimentation

Figure 4.2 exhibits the different modes of sedimentation during the experiments.

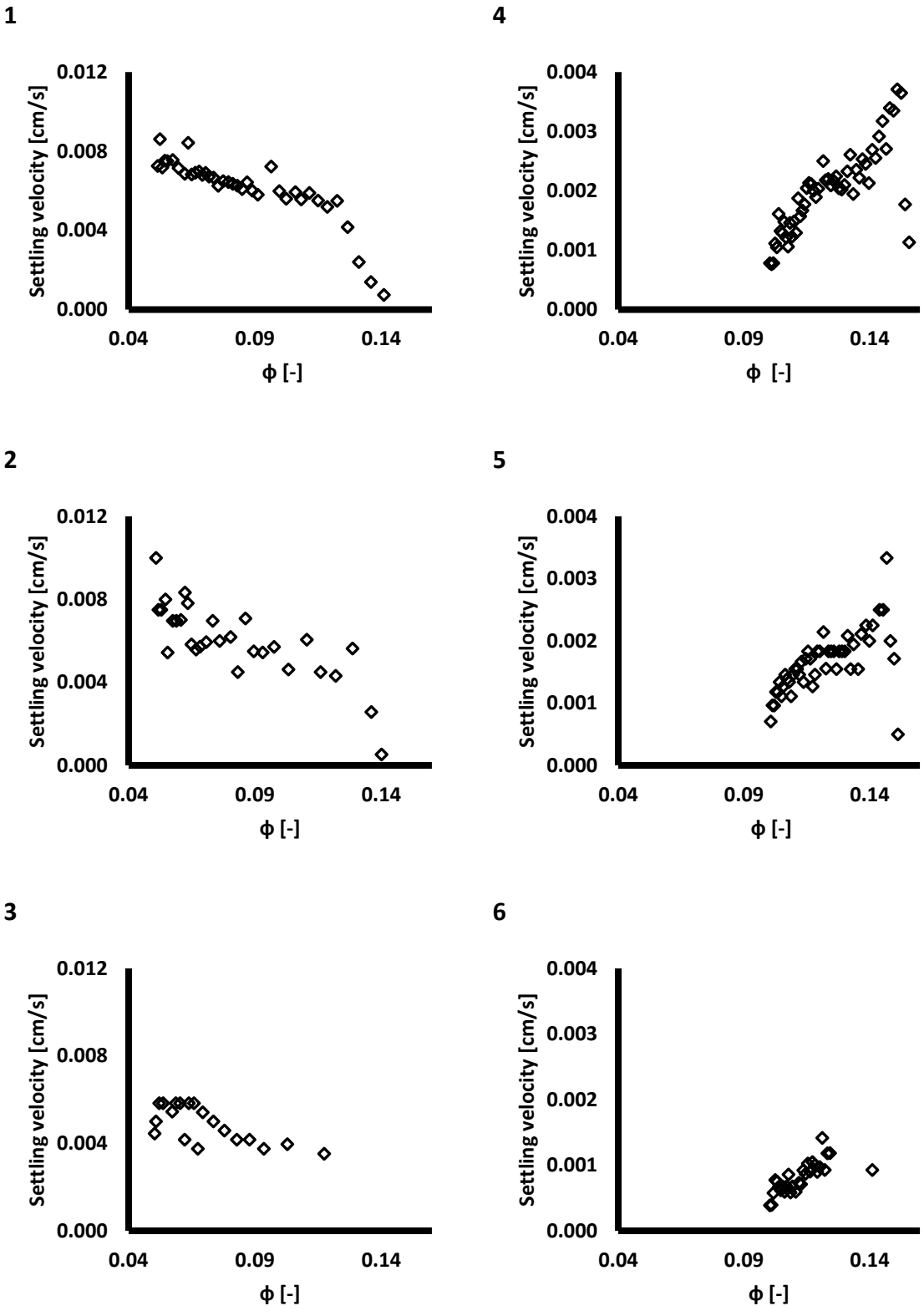

Figure 4.2. ***1:*** *pH=2.9 & Vol. 5% ;* ***2:*** *pH=6.7 & Vol. 5%;* ***3:*** *pH=9.4 & Vol. 5%;* ***4:*** *pH=2.9 & Vol. 10%;* ***5:*** *pH=6.7 & Vol. 10%;* ***6:*** *pH=9.4 & Vol. 10%.*

All the data yielded from *set up 1* was processed and each sedimentation profile was obtained as follows:

$$v_S = {\Delta h}/{\Delta t} \tag{22}$$

$$\emptyset = \frac{H\emptyset_0}{h(t)} \tag{23}$$

Figure 4.2 shows each sedimentation profile depending on both, the concentration and the pH level. Additionally, it could be observed some dispersed points during the sedimentation process within the lower cellulose concentration slurries. Most likely, all of them are thought to be as a result of either an improper stirring or even an incorrect filling of the cell. In contrast, a hindered settling due to the increased interaction among all particles is supposed to be for high cellulose concentration slurries.

4.2.3 Hindered settling rates

Considering Richardson and Zaki's approach (16), using a particle diameter according to the average diameter measured by laser diffraction for the high pH slurry is obtained the hindered settling velocity showed in *Fig. 4.3*. It was taken a sphere whose diameter was according to particle characterization for high pH slurries, in which concentration effects are much higher as a result of the mentioned distorted double layer. Afterwards, the terminal velocity or Stoke's velocity was calculated from (1).

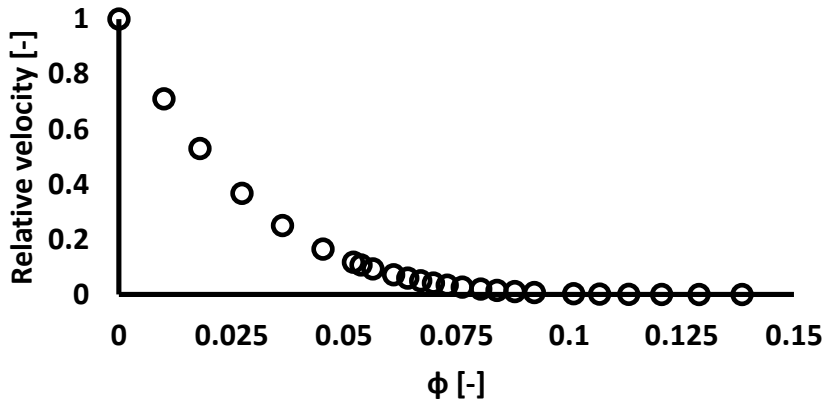

Figure 4.3. Richardson and Zaki's profile: a single sphere falling downwards depending on concentration effects.Relative velocity is obtained as follows: u/u_{St}

From *Figure 4.3* can be observed that concentration effects become important even at very low concentrations.

The settling velocity was compared between the observed velocity from the real suspension and the Stoke's velocity approach for a single sphere (*Fig. 4.4*). A simple ratio is defined by i.e.

$$u_r = {}^{u_s}/_{u_{st}} \tag{24}$$

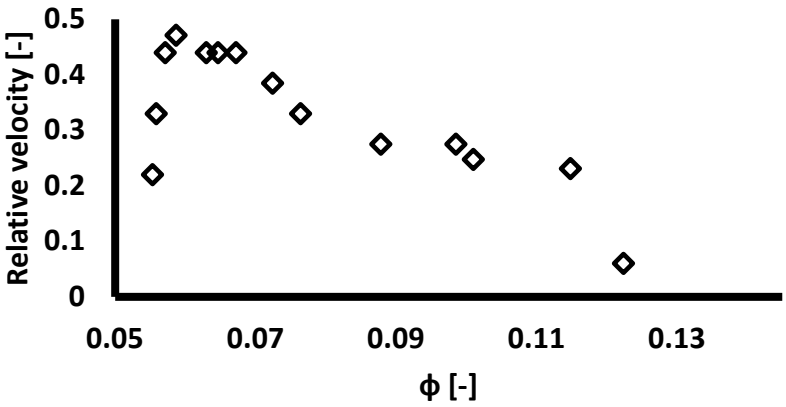

Figure 4.4. Relative velocity for low solid concentration and high pH.

It is observed (*Fig. 4.4*) that the terminal velocity for the real suspension reaches almost half of the Stoke's velocity at low ϕ. Afterwards the settling rate decreases as ϕ increases owing to hindered effects such as the distorted double layer become stronger and stronger within the sedimentation process. As *Figure 4.4* exhibits, the initial points correspond at the particles acceleration due to hindered effect is not displayed yet.

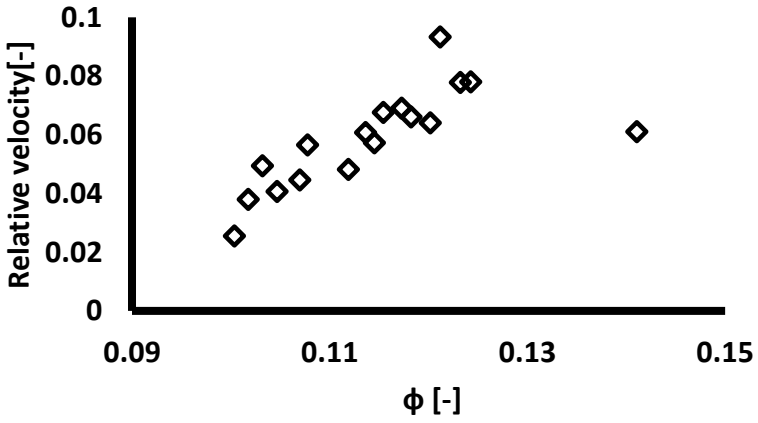

Figure 4.5. Relative velocity for high solid concentration and high pH.

In contrast, for high concentration (*Fig. 4.5*) it could be seen that the inertia of the cluster of particles should be taken under consideration due to their constant acceleration during time. Finally, the suspension ends up over a critical solid concentration which does not allow reaching the terminal velocity in the time frame of the process. The agglomerates only reach about 10% of Stoke's velocity.

Overall, these conclusions discussed before from *Figures 4.4* and *4.5* could be applicable for the other cases whose results came out to be in the same extent (*Fig. 4.3*).

4.3 Solid volume fraction

Solid volume fraction was calculated by Lambert-Beer's equation (21) for *set up 2*. The following sections show the results obtained after processing the data.

4.3.1 Column profile

Figures 4.6 and *4.7* display the spatial distributions of solid fractions in the final sediment of each slurry. Once each sediment was built up, the next step in the procedure followed: the column was checked to measure the solid volume fraction at specific heights indicated below in *Figure 4.6* and *Figure 4.7.*

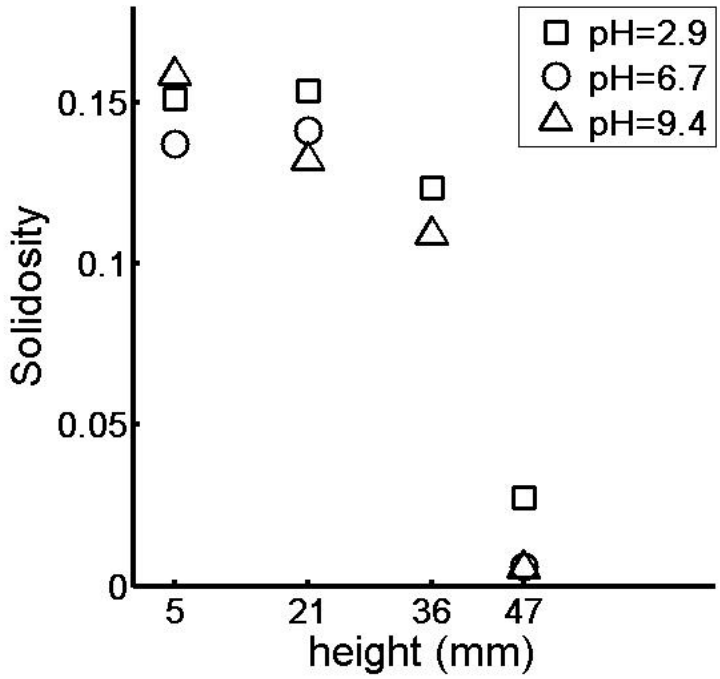

Figure 4.6. End profile (low concentration). The following heights were chosen (from bottom to top): 5 mm, 21 mm, 36 mm and 47 mm. The last one is placed 7 mm above the upper sediment surface.

The cell profile exhibits different solid fraction values along the entire cell from bottom to top; it means that the sediment built up behaves as a compressible sediment. It is observed in *Figure 4.6* for the high-pH slurry that the sediment becomes more compressible but not for the other two kinds of slurries. It might be due to agglomerates settle randomly causing a low polydispersity throughout the sediment.

Moreover, a rather low solid volume fraction, around 0.025, persisted above the formed sediment. Based on visual observation, these particles were considered to consist of some smaller agglomerates waving above the top of the sediment. It might be that the drag and

buoyant forces opposed motion downwards owing to a change in particle size varying particle density; the moisture degree increases leading to a lower particle density that allows remaining in suspension. As the particles became smaller the random movement became more rapid and gave rise to the phenomenon known as Brownian motion. The lower size limit is due to diffusional broadening (or Brownian diffusion) and this diffusion arises from bombardment by fluid molecules which causes the particles to move about in a random manner with displacements in all directions, which ultimately exceed the displacements due to gravity.

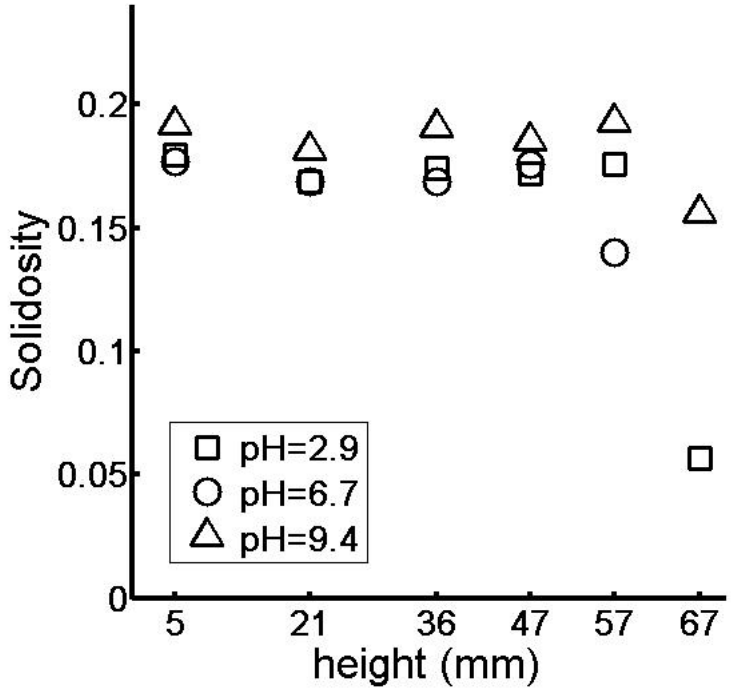

Figure 4.7. End profile (high concentration). The following heights were chosen (from bottom to top): 5 mm, 21 mm, 36 mm, 47 mm, 57 mm and 67 mm. The last one is placed 2 mm above the upper sediment surface.

In contrast to *Figure 4.6, Figure 4.7* exhibits a step like profile. A hypothesis might be that the sediment becomes a compact, networked structure so that less sparse regions. In other words, the solid volume fraction of the sediment slightly increased from top to bottom for all three slurries in the same extent.

It is thought, however, flocculation leads to bulky sediment that contains more interstitial water in sediment as it happens at low and neutral pH slurries.

4.3.2 Local solidosity during sedimentation process

During sedimentation experiments, a fixed height (5 mm) was chosen so as to follow the solid volume fraction variations as a function of time by ϒ-rays measurements. These results are displayed in *Figure 4.8* and *Figure 4.9*.

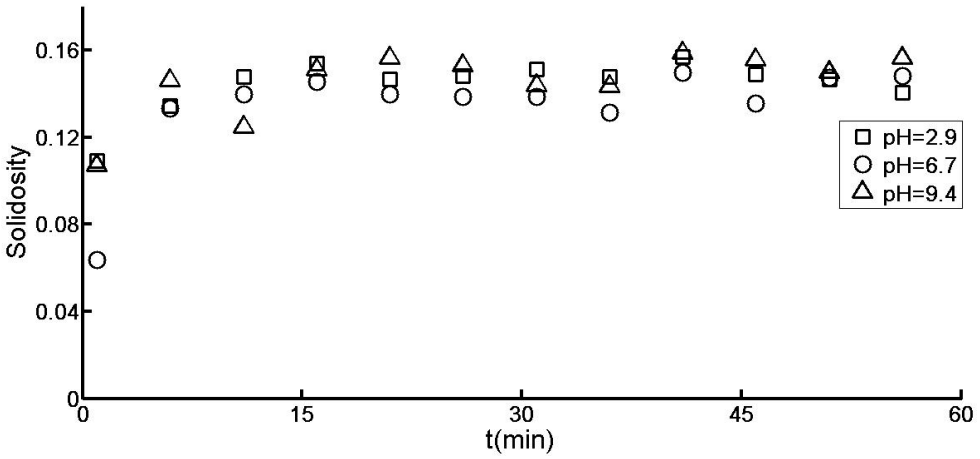

Figure 4.8. Initial sedimentation process (low solid concentration).

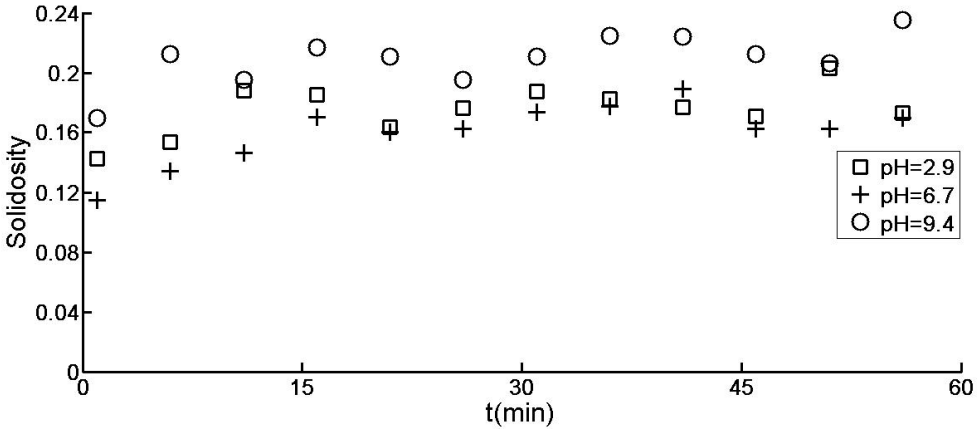

Figure 4.9. Initial sedimentation process (high solid concentration).

It can be observed that the high pH has a higher solidosity compared with the lower pHs at a given time and initial concentration.

The experimental error is estimated to be ±0.03 in absolute units based on older experimental results which used the same apparatus and material.

4.3.3 Compressible sediment

Theoretically, the average solid volume fraction could be calculated from a material balance:

$$\emptyset(h_{Final}) = \frac{H\emptyset_0}{h(t_\infty)} \tag{25}$$

But in fact, the theoretical solid volume fraction is estimated for the uppermost sediment layer only. In contrast, the experimental solid volume fraction was measured by means of ϒ-attenuation in a fixed height placed 5 mm from bottom of *set up 2* and displayed in *Figures 4.3* and *4.4*.

The theoretical and the calculated solid volume fraction are all given in *Table 4.1*.

Table 4.1.Solid volume fraction. The theoretical solidosity (average) was taken from the uppermost sediment layer at a time estimated to be (t_∞) and the experimental solidosity (local solidosity) was taken from 5 mm from bottom of set up 2.

	5% Vol. concentration		10% Vol. concentration	
pH	**$\phi(h(t_\infty))_{THEORETICAL}$**	**$\phi_{EXPERIMENTAL}$**	**$\phi(h(t_\infty))_{THEORETICAL}$**	**$\phi_{EXPERIMENTAL}$**
2.9	0.14	0.14	0.15	0.18
6.7	0.15	0.15	0.15	0.18
9.4	0.14	0.16	0.15	0.19

The same concentration throughout all the sediment is expected for non-compressible sediments. It exists a slightly difference between each other, though. Comparing both results, and as in *section 4.2.1* was presented, a concentration gradient exists. It is most likely that the sediment could be compacted due to the local solid pressure.

4.3.4 Solid local pressure

The local solid pressure equation takes the form:

$$P_S = \int_0^z \Delta\rho g \emptyset \partial z \tag{26}$$

Where P_S is the local solid pressure; g is the gravitational acceleration; $\Delta\rho$ is the density difference between the solid phase (s) and the liquid phase (l); and z the vertical distance from the coordinate positioning downward with its origin located at the top of sediment whose corresponding solid fraction is the gel point ϕ_g.

Figures 4.10, 4.11 and *4.12* were obtained according to equation (26). As far as the results are concerned, the local solid pressure could be compared among the different slurries and from the bottom of the column to top.

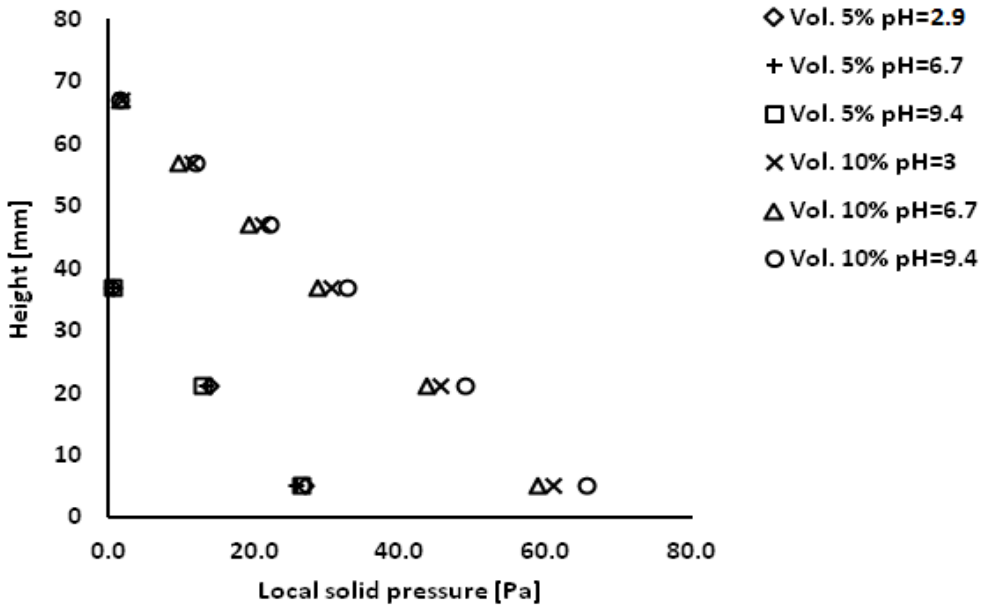

Figure 4.10. Local solid pressure vs column height.

Figures 4.11 and *4.12* exhibit the compressibility for each sediment.

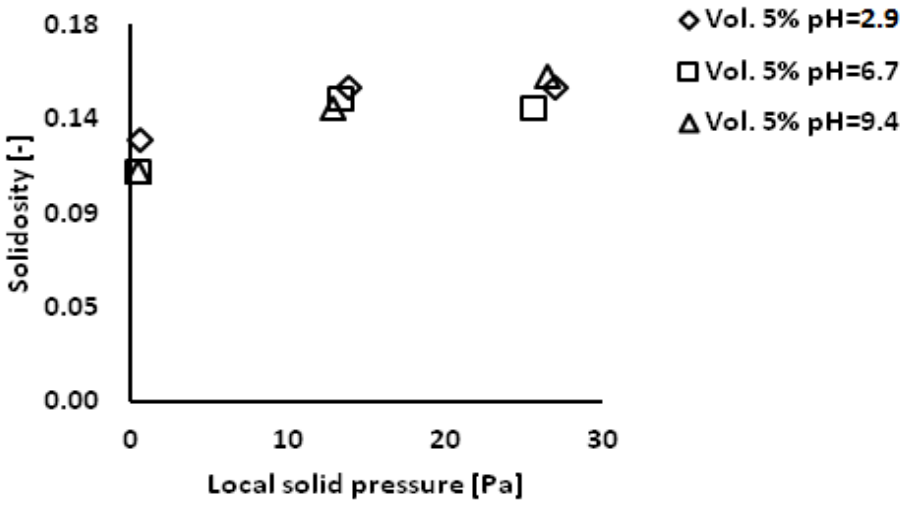

Figure 4.11. Local solid pressure at low concentration vs solidosity.

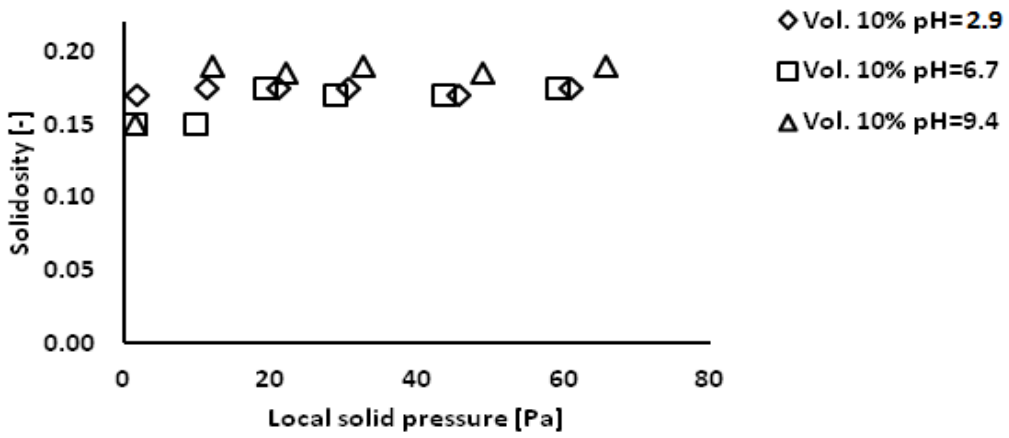

Figure 4.12. Solid local pressure at high concentration vs solidosity.

The following equation makes a proper approach to the compressibility behaviour. It derives from the theory presented by Buscall and White [27].

$$\emptyset = \emptyset_g \left(\frac{P_S}{P_y}\right)^{\beta} \tag{27}$$

P_y is here yet is equal to 1 Pa.

Afterwards, the expression can be rewritten as:

$$ln(\emptyset) = ln(\emptyset_g) + \beta ln\left(P_S/P_y\right) \tag{28}$$

Where ϕ_g is considered to be the null-stress solid volume fraction displayed onto the uppermost layer of the sediment (also named gel point) and P_S is the local solid pressure. Finally, β is a dimensionless parameter which indicates the compressibility of the named sediment built up during the experiment. The β parameter is estimated by fitting *Eq. 28* to the experimental data.

Table 4.2 gathers each β value depending on the different conditions investigated.

Table 4.2. Estimated β parameters in equation (27).

β	pH=2.9	pH=6.7	pH=9.4
Vol. 5%	0.0073 (R^2=0.97)	0.0090 (R^2=0.92)	0.0113 (R^2=0.98)
Vol. 10%	0.0009 (R^2=0.20)	0.0076 (R^2=0.70)	0.0193 (R^2=0.80)

According to *Table 4.2*, the highest β values were reached for the high-pH slurries. It might be due to their internal network that offered less resistance against compacting forces such as the local solid pressure. Meanwhile, the lower β values were reached for the high-concentration-slurries which it means that the sediment offered more resistance against the compacting forces and could not be much more compacted anymore applying the pressures ranged. Hence, high-concentration-and-low-pH sediment can be considered incompressible due to its β value, the lowest.

Regarding the low regression value for the high concentration and low pH is due to its sediment exhibited an uncompressible behaviour. Hence, it could be concluded that $\phi \approx \phi_g$ throughout the entire sediment.

5 Conclusions

Based on the results obtained in this work the following conclusions can be drawn:

- The sedimentation behaviour is affected by the surface charge of the MCC particles.
- Solidosity of the sediment is as a function of pH.
- Compressibility of the sediment was affected by the surface charge of the MCC particles.

6 Future work

It would be useful performing investigations about particle surface properties for MCC particles depending on cristallinity degree and particle size and shape so as to enhance the knowledge about its behaviour.

One more aspect that could be interesting to investigate further is the internal network related with the local solidosity within the sediment varying the surface charge. This work only tried to give a brief overview about the local solidosity, though.

7 Nomenclature

CD	The drag coefficient [-]
d	Particle diameter [m]
d_y	Inner diameter of the *set up 2* cell [m]
F_D	Drag force [N]
f_{bk}	Kynch's batch flux density function [m/s]
g	Acceleration of gravity [m/s^2]
h	Height [m]
H	Total cell height [m]
I	Emerging light flux from the filled *set up 2* cell [cd]
I_0	Emerging light flux from the empty *set up 2* cell [cd]
m	Mass of the particle [kg]
m'	Mass of the fuid [kg]
n	Parameter [-]
n'	Parameter [-]
P_S	Local solid pressure [Pa]
P_y	Yield stress [Pa]
k	Dynamic compressibility [-]
t	Time [s]
t_∞	Final time [s]
U	Buoyant force [N]
u	Particle velocity [m/s]
u_{St}	Stokes's particle velocity [m/s]
u_∞	Theoretical terminal velocity of the particle [m/s]
v_S	Superficial velocity of solids in the z direction [m/s]
v_0	Theoretical terminal superficial velocity of solids in the z direction [m/s]
W	Gravitational force [N]

7.1 Greek letters

β	Parameter [-]
η_γ	Number of counts of the filled *set up 2* cell [-]
$\eta_{\gamma,0}$	Number of counts of the empty *set up 2* cell [-]
μ	Viscosity of the fluid [Pa s]
$\mu_{\gamma,l}$	Attenuation coefficient of the liquid phase [m^{-1}]
$\mu_{\gamma,s}$	Attenuation coefficient of the solid phase [m^{-1}]
ρ_f	Liquid density [kg/m^3]
ρ_s	Solid density [kg/m^3]
ϕ	Local solid volume fraction, solidosity [-]
ϕ_g	Gel point [-]
ϕ_0	Initial solidosity [-]
ϕ_{max}	Maximum solidosity of the sediment [-]

8 Annex

Both sections present the Matlab functions used during the analysis of the data provided from the laboratory.

8.1 Function *Sedimentation*

```
function sedimentation
hold on

seq=5;
d=.06;%m
LTCal=296.9;%5 min
LTExp=59.8*seq;%1 min
mul=19.8;%m
mus=28.9;%m

for z=1:2
%NET=load('lowCpH.m');ny0=514908/LTCal;
%NET=load('lowCpHneutral.m');ny0=510428/LTCal;
%NET=load('LowChighpH2.m');ny0=497327/LTCal;
%NET=load('HighClowpH.m');ny0=506666/LTCal;
if z==1
NET=load('HighCpHneutral.m');ny0=499673/297.1;
t=length(NET);
serie1=zeros(1,t/seq);
s1=ones(1,t/seq);
elseif z==2
NET=load('HighCpH.m');ny0=506666/LTCal;
t=length(NET);
serie2=zeros(1,t/seq);
s2=ones(1,t/seq);
end
A=diag(NET);
m=zeros(1,t/seq);
k=zeros(1,t/seq);
ny=zeros(1,t/seq);
o=zeros(1,t/seq);
for n=1:(t/seq)
m(1)=1;
k(1)=seq;
m(n+1)=m(n)+seq;
k(n+1)=k(n)+seq;
end
for i=1:(t/seq)
r=m(i):k(i);c=m(i):k(i);
A(r,c);
Af=A(r,c);
a=diag(Af);
NETf=sum(a);
ny(i)=NETf/LTExp;
o(i)=((-((log(ny(i)/ny0))+mul*d))./((mus-mul)*d));
if z==1
```

```
serie1(i)=o(i)*s1(i);
elseif z==2
serie2(i)=o(i)*s2(i);
end
end
time=1:seq:990;
subplot(1,2,1)
plot(time,o,'ks')
axis([0 60 0.1 0.3])
xlabel('t(min)');
ylabel('Solidosity');
legend('pH=3','pH=6.7','pH=9.4');
end
obs=serie1-serie2;
P=signrank(obs);
end
```

8.2 Function *Profile*

```
function profile
hold on

%%%lowCpH
%data=[1747210 1944058 1958893 2074531; 3589.3 3587.9 3587.8 3587.1;
514908 573198 568146 570994; 296.9 296.5 296.5 296.5];
%NETexp=[2592 2807 2848 2950; -2592 -2807 -2848 -2950];

%%%lowcphneutral
%data=[1745161 1953028 2109772 2096504; 3589.3 3588 3587 3587.1;
510428 571878 2071301 570384; 296.9 296.5 1187.6 296.5];%netexp LT
netcal LT
%NETexp=[2566 2753 2882 2898; -2566 -2753 -2882 -2898];

%%%lowChighpH
%data=[1680766 1874938 1899699 1996823; 3589.4 3588.1 3588.1 3587.2;
497327 546503 546769 543325; 296.9 296.6 296.6 296.6];
%NETexp=[2625 2828 2850 2966 ; -2625 -2828 -2850 -2966];

%%%highClowpH
%data=[1692974 1887226 1878993 1871438 1877017 1987695; 3589.5 3588.2
3588.2 3588.2 3588.2 3587.4; 506666 561093 560411 557479 560221
556014; 296.9 296.6 296.6 296.6 296.6 296.6];
NETexp=[2629 2810 2829 2846 2859 2972; -2629 -2810 -2829 -2846 -2859 -
2972];
%%%highCpHneutral
%data=[1670591 1872749 1869022 1856250 1893076 2044153; 3589.5 3588.3
3588.3 3588.2 3588.2 3587.2; 499673 557273 556028 554383 554534
550983; 297.1 296.8 296.8 296.8 296.8 296.8];
%%%highCpH
data=[1681334 1873608 1861789 1857791 1859043 1882641;3589.5 3588.2
3588.2 3588.2 3588.2 3588.0; 506666 561093 560411 557479 560221
556014; 296.9 296.6 296.6 296.6 296.6 296.6];
%NETexp=[2636 2845 2869 2893 2904 2922; -2636 -2845 -2869 -2893 -2904
-2922];
t=length(data);
ny=zeros(1,t);
ny0=zeros(1,t);
```

```
o=zeros(1,t);
ny_upper=zeros(1,t);
ny_lower=zeros(1,t);
o_upper=zeros(1,t);
o_lower=zeros(1,t);
data_upper_exp=zeros(1,t);
data_lower_exp=zeros(1,t);
d=.06;%m
mul=19.8;%m
mus=28.9;%m


for n=1:t
   ny(n)=data(1,n)/data(2,n);
   ny0(n)=data(3,n)/data(4,n);

   o(n)=((-((log(ny(n)/ny0(n)))+mul*d))/((mus-mul)*d));

   data_upper_exp(n)=data(1,n)+NETexp(1,n);
   data_lower_exp(n)=data(1,n)+NETexp(2,n);

   ny_upper(n)=data_upper_exp(n)/data(2,n);
   ny_lower(n)=data_lower_exp(n)/data(2,n);

   o_upper(n)=((-((log(ny_upper(n)/ny0(n)))+mul*d))/((mus-mul)*d));
   o_lower(n)=((-((log(ny_lower(n)/ny0(n)))+mul*d))/((mus-mul)*d));

end

%vector_height=[5 21 36 47];
%vector_height=[5 21 36 47 57 67];

subplot(1,2,1)
plot(vector_height,o,'ks')
legend('pH=3','pH=6.7','pH=9.4');
axis([0 70 0 0.25],'square')
xlabel('height (mm)');ylabel('Solidosity');


subplot(1,2,2)
BOX=[o_upper; o; o_lower];
boxplot(BOX)
axis([0 4 0 0.2],'square');

end
```

9 References

[1] G.J.KYNCH, *A theory of sedimentation*, Department of Mathematical Physics, The University, Birmingham, (1951).

[2] T. MATTSSON, *Investigation of hard-to-filter materials-Relating local filtration properties to particle interaction*, Forest products and Chemical Engineering, Department of Chemical and Biological Engineering, Chalmers University of Technology, Gothenburg (2010).

[3] T. ALLEN, *Particle size measurement vol. 1, Powder sampling and particle size measurement*, CHAPMAN & HALL, Fifth edition (1997).

[4] N. GRALÉN, *Sedimentation and diffusion measurements on cellulose and cellulose derivatives*, Uppsala University, (1944).

[5] T. F. TADROS, *The effect of polymers on dispersion properties*, ICI Plant Protection Division, ACADEMIC PRESS (1982).

[6] T. COSGROVE, *Colloid Science: Principles, Methods and Applications. Effect of polymers on colloid stability*, OXFORD, (2005).

[7] S. DIEHL, *Estimation of the batch-settling flux function for an ideal suspension from only two experiments*, Centre for Mathematical Science, Chemical Engineering Science (2007).

[8] R. BÜRGUER, F. CONCHA, F.M. TILLER, *Applications of the phenomenological theory to several published experimental cases of sedimentation processes*, Chemical Engineering Journal (2000).

[9] J.F.RICHARDSON, W.N. ZAKI, *The sedimentation of a suspension of uniform spheres under conditions of viscous flow*, Department of Chemical Engineering, Imperial College, Chemical Engineering Science (1954).

[10] W. NOCON, *Practical aspects of batch sedimentation control based on fractional density changes*, Powder technology, (2010).

[11] R. BÜRGER, E.M. TORY, *On upper rarefaction waves in batch settling*, Powder technology (2000).

[12] P. GARRIDO, R. BURGOS, F. CONCHA, R.BÜRGER, *Settling velocities of particulate systems*, International Journal of Mineral Processing, ELSEVIER (2004).

[13] D. R. LESTER, S. P. USHER, P. J. SCALES, *Estimation of the hindered settling function from batch-settling tests*, Wiley Interscience, (2005)

[14] R. BÜRGER and W. WENDLAND, *Sedimentation and suspension flows: historical perspective and some recent developments*, Journal of Engineering Mathematics, (2001).

[15] A. C. O'SULLIVAN, *Cellulose: the structure slowly unravels, Department of Chemistry of Agriculture and Forestry Sciences*, University of Wales, (1996).

[16] R. EK, G. ALDERBORN, C. NYSTRÖM, *Particle analysis of microcrystalline cellulose: Differentiation between individual particles and their agglomerates*, International journal of pharmaceutics, ELSEVIER (1994).

[17] C.C. HARRIS, P. SOMASUNDARAN and R.R. JENSEN, *Sedimentation of Compressible materials: analysis of batch sedimentation curve*, Henry Krumb School of Mines, Columbia University, New York, Powder Technology (1975).

[18] A.D. MAUDE and R.L. WHITEMORE, *A generalized theory of sedimentation*, Department of Mining and Fuels, University of Nottingham, (1958).

[19] J. ARAKI, M. WADA, S. KUGA, T. OKANO, *Flow properties of microcrystalline cellulose suspension prepared by acid treatment of native cellulose*, Department of Biomaterials Sciences, The University of Tokyo, ELSEVIER (1998).

[20] K. STANA-KLEINSCHEK and V. RIBITSCH, *Electro kinetic properties of processed cellulose fibers*, Colloids and surfaces, ELSEVIER (1998).

[21] K. STANA-KLEINSCHEK, T. KREZE, V. RIBITSCH and S. STRNAD, *Reactivity and electro kinetical properties of different types of regenerated cellulose fibres*, Colloids and surfaces, ELSEVIER (2001).

[22] A. BISMARCK, J. SPRINGER, A.K. MOHANTY, G. HINRICHSEN and M.A. KHAN, *Characterization of several modified jute fibers using zeta-potential measurements*, Colloid Polym, SPRINGER-VERLAG (2000).

[23] M. ELIMELECH, W. H. CHEN and J.J. WAYPA, *Measuring the zeta (electrokinetic) potential of reverse osmosis membranes by a streaming potential analyzer*, Department of Civil and Environmental Engineering, ELSEVIER (1993).

[24] E. DORN, *Electrokinetic phenomena*, Chem. Catal. (1934).

[25] K. STANA-KLEINSCHEK, S. STRNA and V. RIBITSCH, *Surface Characterization and Adsorption Abilities of Cellulose Fibers*, Institute of Textile Chemistry, University of Maribor, and Institute of Physical Chemistry, Karl Franzens University, POLYMER ENGINEERING AND SCIENCE Vol.39 (1999).

[26] C.P. CHU, D.J. LEE and J.H. TAY, *Gravitational sedimentation of flocculated waste activated sludge,* Department of Chemical Engineering, National Taiwan University, PERGAMON (2001).

[27] R. BUSCALL and L.R. WHITE, *The consolidation of concentrated suspensions. Part I: the theory of sedimentation.* J. CHEM SOC FARADAY TRANS (1987).

[28] Y. T. SHIH, D. GIDASPOW and D.T. WASAN, *Sedimentation of Fine Particles in Nonaqueous Media.* Department of Chemical Engineering, Illinois Institute of Technology, Chicago (1986).